Spectroscopic Measurement of Diffusion Kinetics through Subnanometer and Larger Al_2O_3 Particles by a New Method: The Interaction of 2-Chloroethylethyl Sulfide with γ-Al_2O_3

Sunhee Kim,[†] Oleg Byl,[†] Jin-Chen Liu,[†] J. Karl Johnson,[‡,§] and John T. Yates, Jr.*[,†]

Surface Science Center, Department of Chemistry, University of Pittsburgh, Pittsburgh, Pennsylvania 15260, Department of Chemical Engineering, University of Pittsburgh, Pittsburgh, Pennsylvania 15260, and National Energy Technology Laboratory, Pittsburgh, Pennsylvania 15236

Received: December 5, 2005; In Final Form: March 8, 2006

A new method to study the diffusion properties of molecules into porous materials using transmission IR spectroscopy is employed. A measurement of the diffusion of the 2-chloroethylethyl sulfide (2-CEES) molecule into two types of γ-Al_2O_3 powder is performed, showing that the diffusion rate into subnanometer crystallite particle size γ-Al_2O_3 powders (subnano-Al_2O_3) is higher than that into the larger crystallite particle size powder. It is shown that a surface diffusion mechanism can be used to model the diffusion process giving good agreement with the experimental results, where $D_{\text{subnano-Al}_2\text{O}_3}$ is ∼5 times larger than $D_{\text{multinano-Al}_2\text{O}_3}$ at 170 K for the 2-CEES molecule.

I. Introduction

We introduce in this paper a new experimental method to measure the rate of diffusion of an adsorbable molecule into a packed bed of adsorbent particles. We specifically address the diffusion of the 2-chloroethylethyl sulfide (2-CEES) molecule into packed beds of two types of γ-Al_2O_3 powder that are of subnanometer crystallite particle size (subnano-Al_2O_3) and much larger crystallite particle size (multinano-Al_2O_3). The 2-CEES molecule is a simulant for mustard blister agents having both a sulfur functional group and a chlorine functional group.[1,2]

The reaction kinetics of the mustard molecule (2,2'-dichloroethyl sulfide) with nanosize MgO was studied in the liquid phase using magic angle spinning NMR (MAS-NMR).[3] It was reported that the reaction rate is governed by physical properties of the liquid phase such as liquid surface tension, viscosity, and vapor pressure as well as the reactivity with the MgO surface.

The pulsed field gradient NMR (PFG-NMR) method has been used to investigate the self-diffusion of organic molecules into nanoscale porous materials.[4,5] The diffusivity could be explained by either of two models: the Knudsen diffusion model and the surface diffusion model. It was concluded that the surface diffusion mechanism is the dominant diffusion control process in the nanoscale pore region, and our results reported below confirm this concept.

Partially hydroxylated Al_2O_3 contains a distribution of isolated hydroxyl groups that are capable of hydrogen bonding to adsorbed molecules.[6−8] The formation of hydrogen bonds leads to the loss of the characteristic isolated Al−OH vibrational modes and the formation of associated Al−OH species of lower frequency.[9−11] Transmission IR spectroscopy through a packed bed of Al_2O_3 therefore allows one to witness the diffusion of a molecule into the bed using the isolated Al−OH groups as sensors of the progress of the molecule through the packed bed.

We show that the subnanometer size Al_2O_3 particles are more active in promoting the diffusion of the 2-CEES molecules than the larger particle size Al_2O_3. The relative rate of disappearance of isolated Al−OH groups occurs at lower temperatures for the subnano-Al_2O_3 particles than for the multinano-Al_2O_3 particles, and the concomitant formation of associated Al−OH groups occurs also at lower temperatures for the subnanometer size particles. In addition, comparison of subnano-Al_2O_3 and multinano-Al_2O_3 particles in competitive diffusion studies of 2-CEES at constant temperature shows that the subnano-Al_2O_3 exhibits a higher rate of diffusion.

II. Experimental Section

The equipment used to study the diffusion of an adsorbent molecule into a high-surface-area solid powder consists of a vacuum IR cell[12,13] and a Fourier transform infrared (FTIR) spectrometer. The cell has two KBr windows for transmission of an IR beam, allowing it to pass through the powder held in a supporting W-grid. The base pressure of the vacuum cell is maintained at $\sim 1.0 \times 10^{-8}$ Torr with a turbo-molecular pump.[14] A gas doser is directed toward the sample where, at cryogenic temperature, the incident molecules condense as an ice on the outer geometric surface of the solid powder. The cryogenically cooled manipulator, which holds the powdered sample on the supporting grid within the cell, is movable up and down to observe the spectrum of two different powdered samples, supported one above the other together on the grid. Two different kinds of Al_2O_3 powder sample are pressed into the same W-grid (thickness = 0.005 cm) with a pressure of 70 000 psi. This arrangement allows the diffusion properties of a particular molecule in the two Al_2O_3 samples to be directly compared under exactly the same experimental conditions. The W-grid is suspended between Ni clamps that are connected to Cu leads originating from the manipulator's reentrant Dewar. A type-K thermocouple is welded to the top of the grid.[15] The temperature as measured by the thermocouple, and temperature control is achieved by resistive heating of the W-grid and the powdered samples via the Cu leads using a temperature control program.[12] The resolution of the temperature is 0.1 K in the

* Author to whom correspondence should be addressed. E-mail: jyates@pitt.edu.
[†] Department of Chemistry, University of Pittsburgh.
[‡] Department of Chemical Engineering, University of Pittsburgh.
[§] National Energy Technology Laboratory.

10.1021/jp057075f CCC: $33.50
Published on Web 04/18/2006

TABLE 1: Typical Properties of Two Kinds of Al_2O_3 Powder

	multinano-Al_2O_3	subnano-Al_2O_3
BET surface area (m^2/g)	328	692
BET surface area (m^2/g, our measurement)	392 (354)[a]	777 (463)[a]
pore volume (mL/g)	0.237	1.03
pore volume (mL/g, our measurement)	0.312 (0.282)[a]	1.35 (0.408)[a]
minimum crystallite diameter (nm)[b]	2−3	<1

[a] Compressed with 70 000 psi. [b] The Al_2O_3 crystallite sizes were measured by transmission electron microscopy (personal communication, Dr. Olga Koper, Nanoscale Materials, Manhattan, KS).

range of 83−1400 K. The lower temperature is obtained by cooling the manipulator with liquid N_2.

Powdered γ-Al_2O_3 was obtained from Nanoscale Materials, Inc., Manhattan, KS, and the comparison of the major physical characteristics of two kinds of γ-Al_2O_3 particles is shown in Table 1. The γ-Al_2O_3 with crystallite diameters <1 nm is called subnano-Al_2O_3, and γ-Al_2O_3 with crystallite diameters between 2 and 3 nm is called multinano-Al_2O_3 in this work. The Brunauer−Emmett−Teller (BET) surface area and the pore volume of subnano-Al_2O_3 are higher than those of the multinano-Al_2O_3. Even after powder compression the subnanoparticles still have a higher surface area (463 m^2/g) and pore volume (0.408 mL/g) compared to multinano-Al_2O_3 (354 m^2/g, 0.282 mL/g). The Al_2O_3 powder pressed into the W-grid (after removing the excess with a blade) weighs 3.65 ± 0.14 mg for subnano-Al_2O_3 and 3.40 ± 0.10 mg for multinano-Al_2O_3. Optical microscopy images of the W-grid with the pressed Al_2O_3 powder are shown in Figure 1. The filling of the 0.2 mm × 0.2 mm square windows in the grid is >98%.

After the two alumina samples were annealed (800 K, in vacuum) to produce the isolated Al−OH groups, 2-CEES (g) (supplied as a liquid from Aldrich) is introduced to the Al_2O_3 samples at 126 K to form a condensed film of 2-CEES on their front and back geometrical outer surfaces. All of the spectra of 2-CEES on both of the Al_2O_3 surfaces, following a momentarily programmed increase in temperature, are taken after cooling to 126 K, which is below the 2-CEES freezing temperature. For the isothermal diffusion experiment at 170 K, after the formation of the 2-CEES ice film on the outer geometric surface at 126 K, the sample is annealed at 165 K briefly before heating to 170 K. The change of absorbance in the ν(OH) region is measured using difference spectra referenced to the initial spectrum at 126 K.

The FTIR spectra are collected with a Bruker TENSOR 27 FTIR spectrometer by the transmission method. The spectrometer and the optic enclosures are purged continuously with H_2O- and CO_2-free air. Each spectrum is obtained by averaging 64 interferograms at 2 cm^{-1} resolution.

III. Results

A. Behavior of Isolated Al−OH Groups during 2-CEES Diffusion into the Al_2O_3 Interior. Figure 2 shows the absorbance behavior of the isolated Al−OH groups as 2-CEES is caused to diffuse into the interior of the compressed powder samples by raising the temperature. Up to 175 K, the inward diffusion process occurs from the 2-CEES layer that is crystalline-ice-like, as judged by the IR spectra (to be discussed later) and by a temperature programmed desorption (TPD) experiment (not shown here). The onset of the 2-CEES ice desorption from the outer surface of Al_2O_3 occurs at ~175 K. Above 175 K, 2-CEES inward diffusion continues, and the diffusion process is accompanied by a small amount of desorption from the ice overlayer. It may be seen that the relative rate of entry of 2-CEES into the interior is greater for subnano-Al_2O_3 than that for multinano-Al_2O_3 throughout the experiment. The isolated Al−OH group with its frequency at 3760 cm^{-1} for multinano-Al_2O_3 and at 3740 cm^{-1} for subnano-Al_2O_3 is monitored in each case, and the absorbance of these species decreases upon heating due to hydrogen bonding to 2-CEES. The absorbance changes of ν(OH) are normalized to the change after heating at 240 K for multinano-Al_2O_3 and to 210 K for subnano-Al_2O_3, the temperatures where 2-CEES binding to Al−OH groups is maximized, respectively. Above this temperature in each case the isolated Al−OH groups are restored as a result of extensive desorption of the chemisorbed 2-CEES from the Al−OH trap sites.[11,16]

To constantly maintain an outer layer of crystalline-ice-like 2-CEES during the diffusion process, a second type of diffusion experiment was carried out isothermally at 170 K, where the presence of crystalline-ice-like 2-CEES at the outer geometrical boundary of the powdered Al_2O_3 bed was verified by its IR spectrum throughout the experiment. In a fashion similar to the temperature dependence experiment in Figure 2, the absorbance change of ν(OH) is normalized to that after heating at 240 K

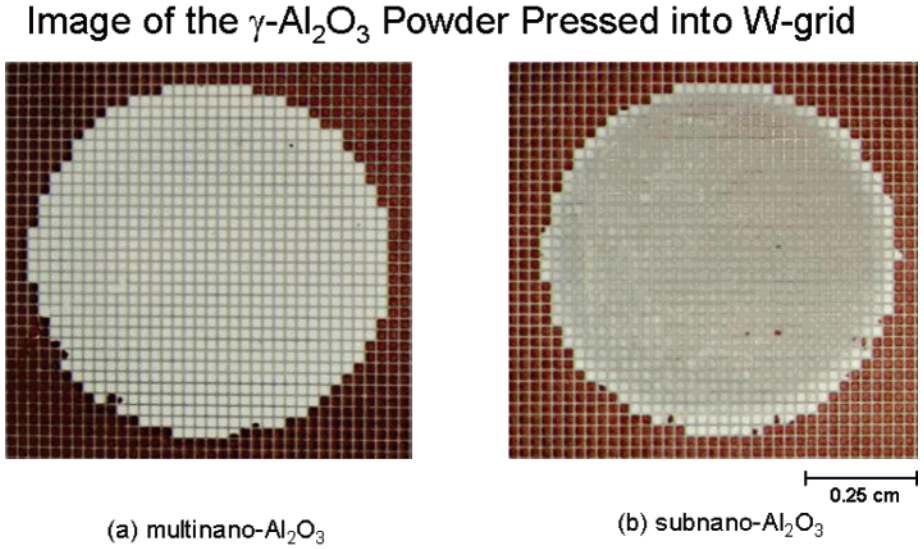

Figure 1. Image of γ-Al_2O_3 powder pressed into a W-grid with a pressure of 70 000 psi for (a) multinano-Al_2O_3 and (b) subnano-Al_2O_3.

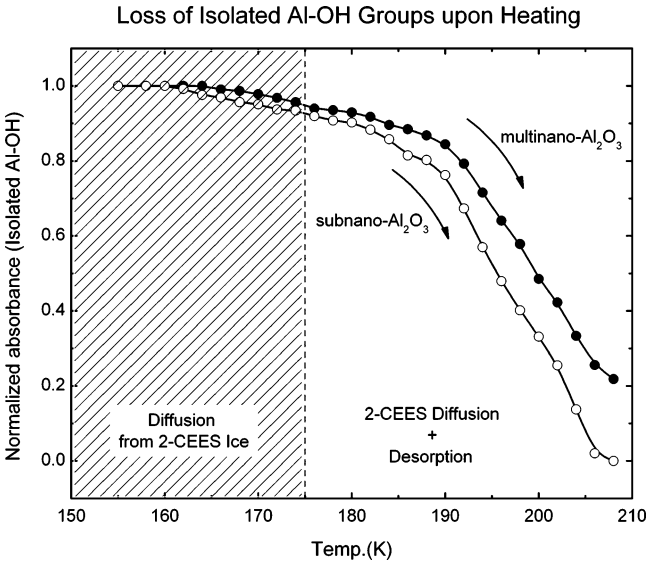

Figure 2. Loss of the normalized absorbance of isolated Al−OH groups at ∼3760 cm^{-1} for multinano-Al_2O_3 (filled circles) and at ∼3740 cm^{-1} for subnano-Al_2O_3 (open circles) upon increasing the temperature. All of the FTIR spectra are measured at 126 K. The absorbance change is normalized by that obtained at higher temperature where 2-CEES binding to Al−OH groups is maximized at 240 K for multinano-Al_2O_3 and at 210 K for subnano-Al_2O_3, respectively.

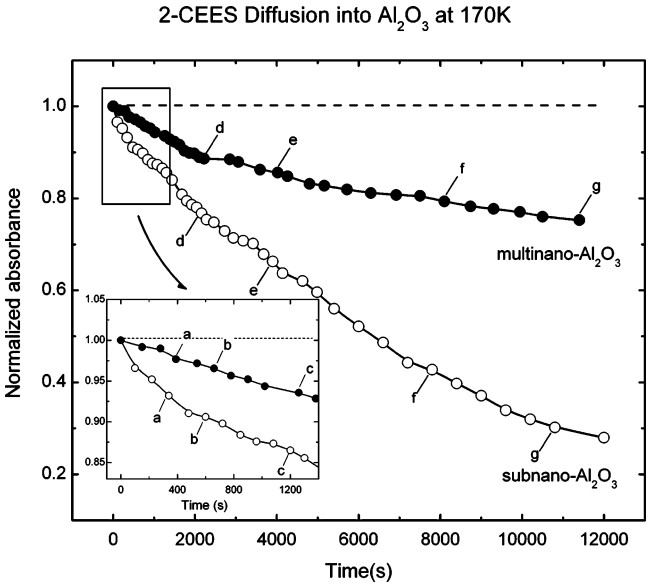

Figure 3. Plot of the loss of the normalized absorbance of isolated Al−OH at ∼3760 cm^{-1} for multinano-Al_2O_3 (filled circles) and at ∼3740 cm^{-1} for subnano-Al_2O_3 (open circles) as a function of heating time at 170 K. A magnified image in the region for 0−1400 s is shown in the lower inset. The absorbance change is normalized by the change obtained after heating the sample at 240 K for multinano-Al_2O_3 and at 210 K for subnano-Al_2O_3. The data points noted as a−g on the multinano-Al_2O_3 curve correspond to those at 390, 660, 1260, 2220, 4020, 8100, and 11 400 s and similarly on the subnano-Al_2O_3 curve correspond to 340, 600, 1200, 2160, 3900, 7800, and 10 800 s. FTIR spectra for these diffusion times are given in Figures 4 and 5.

for multinano-Al_2O_3 and 210 K for subnano-Al_2O_3. (The FTIR spectra during diffusion at 170 K will be shown in Figures 4 and 5.) The results of this experiment are shown in Figure 3, comparing the two types of Al_2O_3. Again it is observed that the subnano-Al_2O_3 exhibits a more rapid relative rate of loss of isolated Al−OH groups, compared to multinano-Al_2O_3. After 1000 s, the fraction of the isolated Al−OH groups consumed on the subnano-Al_2O_3 by hydrogen bonding to 2-CEES is almost

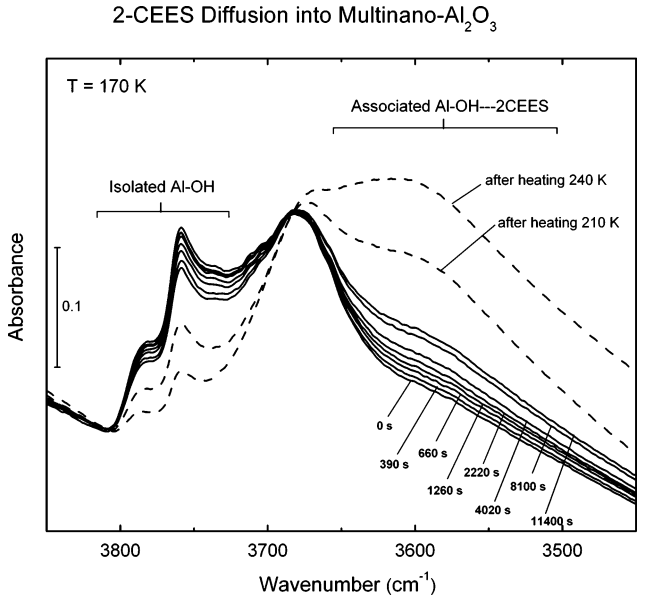

Figure 4. FTIR spectra of 2-CEES on the multinano-Al_2O_3 at 170 K with increasing time in the ν(OH) region. The formation of the 2-CEES ice film is carried out at 126 K.

twice that observed for the multinano-Al_2O_3. By the end of the experiment at 170 K, when 12 000 s of diffusion has occurred, the subnano-Al_2O_3 has, in a relative way, experienced about three times the consumption of Al−OH groups compared to the multinano-Al_2O_3 sample, using the normalized ν(OH) absorbance for this kinetic comparison.

Figure 4 shows the infrared spectrum of multinano-Al_2O_3 during the diffusion of 2-CEES into the interior of the compressed powder at 170 K. Two sharp IR features at ∼3780 and ∼3760 cm^{-1} due to isolated Al−OH groups are observed to disappear monotonically, while a broad associated OH band near 3600 cm^{-1} forms. The broad band is due to hydrogen bonding of the isolated Al−OH groups to the 2-CEES molecule, and this process has been reported previously using another γ-Al_2O_3 material.[11,16] Figure 4 also shows the enhanced loss of isolated Al−OH species from the surface after heating to 210 and 240 K, respectively, where the formation of associated OH groups and the loss of the isolated OH groups has been maximized.

Figure 5 shows the spectral behavior of the isolated Al−OH groups for the subnano-Al_2O_3 sample. In this case, the integrated absorbance in the 3800−3700 cm^{-1} region due to isolated Al−OH species is approximately the same as that in the multinano-Al_2O_3 case compared to the subnano-Al_2O_3 case (note vertical scale change from Figure 4 to Figure 5), and the two Al−OH species observed on the multinano-Al_2O_3 material are not resolved. But in the difference spectra obtained during diffusion (not shown here) one sees clearly that two kinds of Al−OH species are present at ∼3790 and ∼3740 cm^{-1}. Here, the normalized absorbance of these two groups decreases as 2-CEES diffusion occurs into the interior. A broad band, centered near 3600 cm^{-1}, is observed to form as 2-CEES hydrogen-bonds to the isolated Al−OH groups. Figure 5 also shows that the maximized 2-CEES binding to Al−OH is observed at 210 K, followed by partial recovery of the absorbance of isolated Al−OH groups upon heating to 240 K.

B. Spectroscopic Changes in 2-CEES IR Spectra during Diffusion into Al_2O_3. The IR transmission spectrum through the 2-CEES/Al_2O_3 sample is quite informative about the state of the 2-CEES during the diffusion experiment. When 2-CEES is deposited at 126 K, we observe in the C−H stretching region

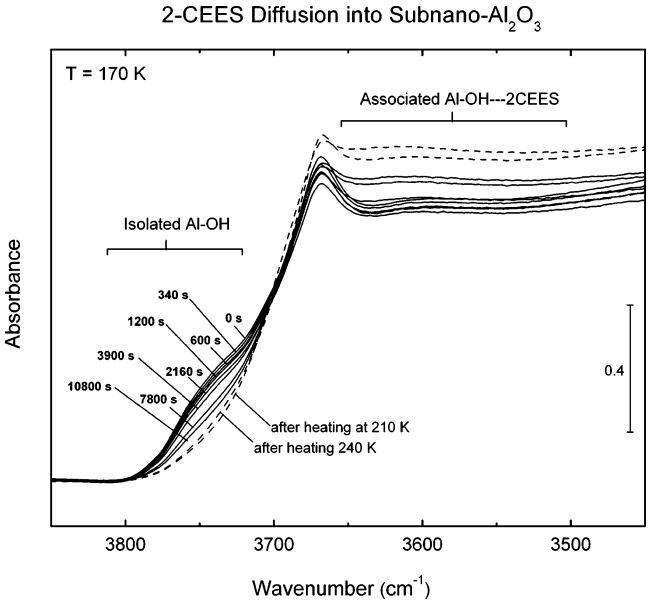

Figure 5. FTIR spectra of 2-CEES on the subnano-Al_2O_3 at 170 K with increasing time in the ν(OH) region. The formation of the 2-CEES ice film is carried out at 126 K.

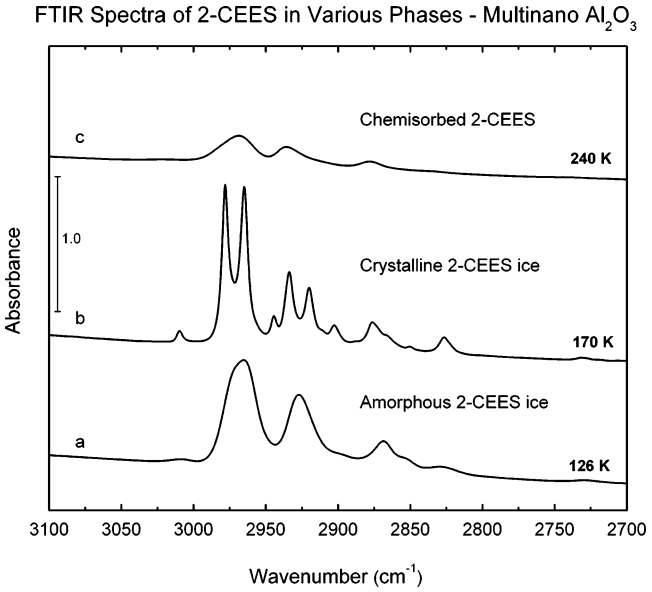

Figure 6. FTIR spectra of 2-CEES on multinano-Al_2O_3 in the ν(C−H) region: (a) in the amorphous condensed phase at 126 K; (b) in the crystalline condensed phase at 170 K; (c) in the chemisorbed phase at 240 K.

a total of seven broad features as seen in Figure 6a. The breadth of the IR features is consistent with the presence of an amorphous 2-CEES ice, produced by condensation at the low temperature. When 2-CEES is heated to 170 K, the spectrum exhibits sharpened bands as seen in Figure 6b, and 11 major features become resolved. This is due to the conversion of an amorphous ice of 2-CEES to a crystalline ice of 2-CEES.[17] We have confirmed this amorphous-to-crystalline ice transformation by observing the same spectral change from amorphous to ice 2-CEES for a bulk condensed sample of 2-CEES in the absence of Al_2O_3. Finally after extensive diffusion of 2-CEES into the Al_2O_3 at 240 K and its chemisorption on interior sites, the broadened spectrum, shown in Figure 6c, is produced. It is noted that the IR spectrum in the C−H stretching region of the fully hydrogen-bonded adsorbed 2-CEES closely resembles that of the amorphous 2-CEES at 126 K, indicating that crystalline

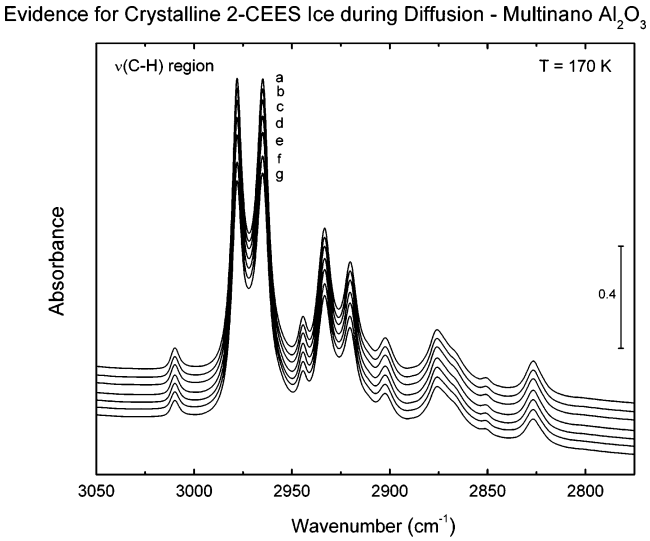

Figure 7. FTIR spectra of 2-CEES on multinano-Al_2O_3 in the ν(C−H) region at 170 K with increasing time. Heating times are 390, 660, 1260, 2220, 4020, 8100, and 11 400 s, which correspond to the points labeled a−g in Figure 3.

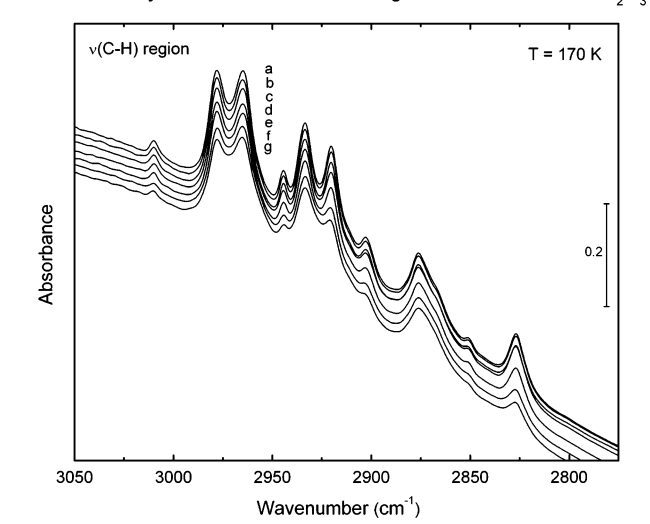

Figure 8. FTIR spectra of 2-CEES on subnano-Al_2O_3 in the ν(C−H) region at 170 K with increasing time. Heating times are 340, 600, 1200, 2160, 3900, 7800, and 10 800 s, which correspond to the points labeled a−g in Figure 3.

ordering of 2-CEES molecules is responsible for the sharp spectrum (Figure 6b) and that the molecular 2-CEES disordering both in the amorphous ice and in the adsorbed layer breaks the crystalline order of the ice.

We employ the observation of the ice 2-CEES spectrum to confirm in the isothermal diffusion measurements at 170 K that the crystalline ice 2-CEES layer is present as a source of diffusing 2-CEES *throughout the experiment*. Thus, in Figure 7, the C−H region displays the 11 major IR bands indicative of the presence of crystalline ice 2-CEES on the multinano-Al_2O_3 sample; in Figure 8, on the subnano-Al_2O_3 sample, we also observe the presence 11 bands indicative of the presence of crystalline ice 2-CEES throughout the entire isothermal diffusion measurements.

IV. Discussion

A. Summary of the Experiments. Experiments similar to that shown in Figure 2 have been reported previously for another

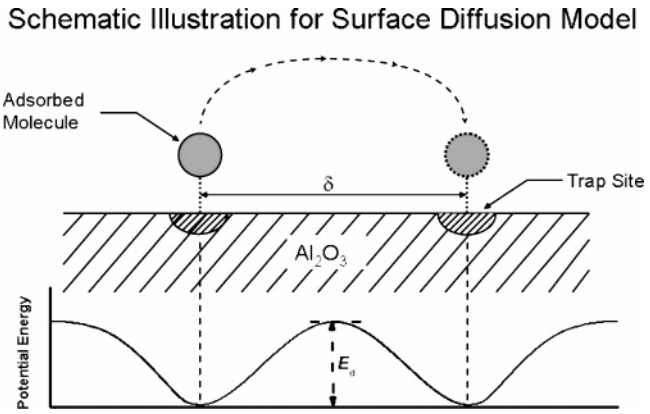

Figure 9. Schematic illustration for surface diffusion model.

γ-Al_2O_3 sample.[11,16] The spectral behavior of the Al−OH features in the previous work for 2-CEES diffusion is essentially identical to that observed for multinano-Al_2O_3 shown in this work. The subnano-Al_2O_3 differs in its hydroxyl IR spectrum due to the different morphology and method of preparation of this very high area material. Judging from the integrated absorbance of the isolated Al−OH groups between 3810 and 3700 cm^{-1}, the two Al_2O_3 materials contain approximately the same number of isolated Al−OH groups per unit mass. It is clear from our diffusion measurements, using Al−OH groups as sensors for the arrival of the 2-CEES molecule, shown in Figures 2 and 3, that the rate of entry of 2-CEES into the interior of the powdered Al_2O_3 is faster for the subnano-Al_2O_3 than for the multinano-Al_2O_3 material. The Al−OH absorbance change measurements (using Al−OH groups as sensors of 2-CEES arrival and trapping) are indicative of the fractional entry of 2-CEES into the powder interior. In addition to Al−OH groups, other types of adsorption sites (such as Lewis acid sites) may also be active for 2-CEES bonding and trapping.[11,16]

The application of these and other γ-Al_2O_3 preparations for sorption processes will involve other molecules at temperatures above the cryogenic temperatures used here. We have employed such low temperatures to slow the diffusion process so that it may be conveniently observed in the laboratory, allowing a comparison of molecular diffusion through subnano- and multinano-particle size sorbents

B. Modeling Diffusion into Al_2O_3 Powders. Porous materials are characterized by pore volume, pore size distribution, pore topology, pore morphology, surface area, surface chemistry, properties of the material, etc. These factors, apart from the properties of the adsorbing fluids, determine the adsorption and diffusion properties of fluids into the materials.

The diffusion of 2-CEES into γ-Al_2O_3 causes the formation of a 2-CEES adsorption complex at the isolated hydroxyl groups and at other types of adsorption sites.[11,16] We call all these sites trapping sites (T-sites) in this paper. Such trapping sites play an important role in the diffusion and adsorption process of 2-CEES into γ-Al_2O_3. We consider the effect of T-sites in controlling the surface diffusion,[18] as shown schematically in Figure 9. Here T-sites are located distance δ from each other, and the activation energy for diffusion, E_d, is determined at the crossover point between the T-sites.

The diffusivity for surface diffusion has the following form

$$D_s = \frac{\delta^2}{6\tau} \tag{1}$$

where δ is the distance between adjacent sites (m) and τ is the average time that a site is occupied between jumps (s). τ is given by

$$\tau = \tau_0 \exp\left(\frac{E_d}{RT}\right) \tag{2}$$

where E_d is the diffusion activation energy (J mol^{-1}), R is the universal gas constant (J mol^{-1} K^{-1}), T is the temperature (K), and $\tau_0 = \delta/V_T$ (s), in which V_T is the thermal velocity of the adsorbate molecule (m s^{-1}). Combining eqs 1 and 2, we have

$$D_s = \frac{1}{6} V_T \delta \exp\left(-\frac{E_d}{RT}\right) \tag{3}$$

If we assume a uniform distribution of the T-sites, then we have

$$\delta \propto \frac{1}{\sqrt{C_{\text{T-sites}}}} \tag{4}$$

where $C_{\text{T-sites}}$ is the concentration of the T-sites (mol m^{-2}).

The diffusivity ratio is given by

$$\frac{D_{s,\text{subnano}}}{D_{s,\text{multinano}}} = \sqrt{\frac{C_{\text{T-sites,multinano}}}{C_{\text{T-sites,subnano}}}} \exp\left(-\frac{(E_{d,\text{subnano}} - E_{d,\text{multinano}})}{RT}\right) \tag{5}$$

If we assume, for both multinano-Al_2O_3 and subnano-Al_2O_3, then

$$\frac{E_a}{E_d} = Q \tag{6}$$

where E_a is the desorption activation energy (J mol^{-1}), E_d is the diffusion activation energy (J mol^{-1}), and Q is constant. The value of Q depends on the surface roughness, the adsorbate size, and the number of bonds made with the substrate. Q is about 2−10 for simple molecules on metal surfaces;[19] for 2-CEES diffusion into γ-Al_2O_3, we assume $Q = 4-8$ in our analysis.

We can estimate the diffusion activation energy from the desorption activation energy, E_a. The latter can be calculated from the results of thermal desorption experiments.[20,21] For first-order desorption, the Redhead equation is

$$\frac{E_a}{RT_p} = \ln\left(\frac{\nu_1 T_p}{\beta}\right) - \ln\left(\frac{E_a}{RT_p}\right) \tag{7}$$

where β is the heating rate (K s^{-1}), ν_1 is the reaction rate constant (s^{-1}), E_a is the desorption activation energy (J mol^{-1}), and T_p is the temperature at which the desorption rate is a maximum (K).

From the experiments we have normalized the absorbance of isolated Al−OH versus temperature for 2-CEES diffusion into the γ-alumina (Figure 2). At low temperatures, the adsorption amount increases with an increase of temperature. The isolated Al−OH groups are consumed, and associated Al−OH groups are formed in this process. At some higher temperature, T_d, the competition between diffusion into the material and desorption out of the material reaches a balance, and the amount of the isolated/associated Al−OH groups reaches a minimum/maximum. From the experiments, T_d is 240 and 210 K for multinano-Al_2O_3 and subnano-Al_2O_3, respectively.

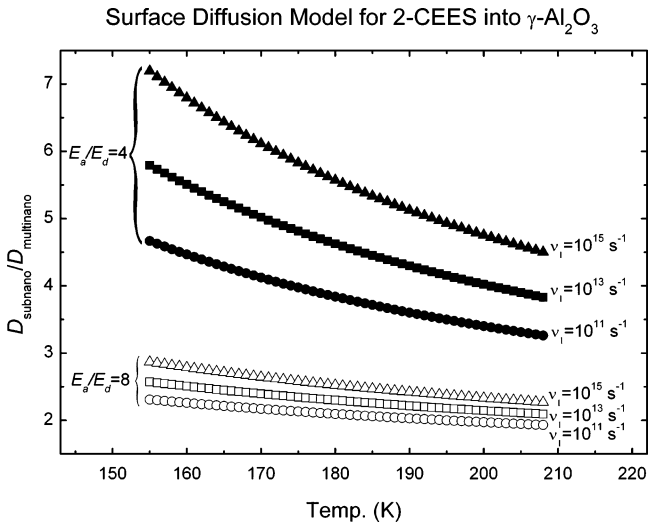

Figure 10. Ratio of the diffusion coefficient for 2-CEES on multinano-Al_2O_3 and subnano-Al_2O_3 modeled by the surface diffusion mechanism.

To estimate the desorption activation energy, we need T_p, the temperature at which the desorption rate is a maximum. Generally, T_p is smaller than T_d. If we assume that

$$T_{p,\text{multinano}} - T_{p,\text{subnano}} = T_{d,\text{multinano}} - T_{d,\text{subnano}} \tag{8}$$

and the desorption activation energy is independent of the coverage, then we can estimate the desorption activation energy from eq 7 as a function of ν_1. Then we can calculate the diffusion activation energy, E_d, as a function of Q from eq 6. The diffusivity ratio can be obtained from eq 5 if we know the T-site concentrations, $C_{\text{T-sites}}$. We have estimated from the integrated absorbance ratio for the isolated OH group on the two types of Al_2O_3 that

$$\frac{N_{\text{T-sites,subnano}}}{N_{\text{T-sites,multinano}}} = \frac{S_{\text{subnano}} C_{\text{T-sites,subnano}}}{S_{\text{multinano}} C_{\text{T-sites,multinano}}} \approx 1 \tag{9}$$

where $N_{\text{T-sites}}$ is the amount of effective T-sites per gram of alumina (mol g^{-1}), S is the specific surface area (m^2 g^{-1}), and $C_{\text{T-sites}}$ is the concentration of the effective T-sites (mol m^{-2}). Thus

$$C_{\text{T-sites,multinano}} = \frac{S_{\text{subnano}}}{S_{\text{multinano}}} C_{\text{T-sites,subnano}} \approx 1.3 C_{\text{T-sites,subnano}}$$

The diffusivity ratios for 2-CEES in subnano-Al_2O_3 and multinano-Al_2O_3 are shown in Figure 10 for several values of ν_1, ranging from 10^{11} to 10^{15} s^{-1}, and for $Q = 4$ and 8. These ranges of ν_1 and Q were chosen to represent typical values. For the parameters given above, the diffusion coefficient of 2-CEES in subnano-Al_2O_3 is about 2−6 times larger than the diffusion coefficient in multinano-Al_2O_3 at 170 K as shown in Figure 10. As seen above, the effect of the chemical binding properties of T-sites as well as surface area and pore volume contribute to the diffusivity into the γ-Al_2O_3 sample. Since here the difference of the diffusion activation energy on two γ-Al_2O_3 powder samples is chosen from the experimental value, T_d, probably it also is affected by the surface morphology property. The comparison of the ν(OH) modes in Figures 4 and 5 shows that more Lewis acid sites are exposed on multinano-Al_2O_3 than on subnano-Al_2O_3, and these sites are also adsorption sites for 2-CEES.[11,16] This might be another reason for the lower diffusivity on multinano-Al_2O_3.

A fit to the data in Figure 3 can be made by modeling the data with Fick's Second Law to obtain an independent measure of the ratio of diffusion coefficients for the two γ-Al_2O_3 powders. The ratio of diffusion coefficients computed from a regression fit can be used as a check on the validity of the analysis presented above. Accordingly, we have modeled the diffusion of 2-CEES into the γ-Al_2O_3 membrane of thickness, l, with Fick's Second Law in one dimension

$$\frac{\partial C(x,t)}{\partial t} = D\frac{\partial^2 C(x,t)}{\partial^2 x} \tag{10}$$

with the following boundary and initial conditions

$$\begin{cases} C(x,t) = C_0 & x = 0,\ t \geq 0 \\ C(x,t) = C_0 & x = l,\ t \geq 0 \\ C(x,t) = 0 & 0 < x < l,\ t = 0 \end{cases} \tag{11}$$

The solution to eq 10 is[22]

$$\frac{C(x,t)}{C_0} = 1 - \frac{4}{\pi}\sum_{n=0}^{\infty}\frac{(-1)^n}{2n+1}\exp\{-D(2n+1)^2\pi^2 t/l^2\}\cos\frac{(2n+1)\pi x}{l} \tag{12}$$

The total amount of 2-CEES that enters the γ-Al_2O_3 at time t is[22]

$$M_t = \int_0^l C(x,t)\,dx = M_\infty\left(1 - \sum_{n=0}^{\infty}\frac{8}{(2n+1)^2\pi^2}\exp\{-D(2n+1)^2\pi^2 t/l^2\}\right) \tag{13}$$

where M_∞ is the total diffusion amount at infinite time (mol g^{-1}), given by

$$M_\infty = M_{t\to\infty} \approx \rho V_{\text{pore}} \tag{14}$$

in which ρ is the density of 2-CEES (mol m^{-3}) and V_{pore} is the pore volume of the γ-Al_2O_3 (m^3 g^{-1}).

Experimental results in Figure 3 are normalized by the adsorption amount at 210 and 240 K for subnano-Al_2O_3 and multinano-Al_2O_3, respectively. We assume that at these temperatures 2-CEES forms a monolayer on the internal surface of the γ-Al_2O_3.

To compare with experimental results, eq 13 can be rewritten as

$$1 - \frac{M_t}{M_N} = 1 - \frac{\rho V_{\text{pore}}}{M_N}\left(1 - \sum_{n=0}^{\infty}\frac{8}{(2n+1)^2\pi^2}\exp\{-D(2n+1)^2\pi^2 t/l^2\}\right) \tag{15}$$

where M_N is the adsorption amount at 210 or 240 K for subnano-Al_2O_3 or multinano-Al_2O_3 (mol g^{-1}). In addition

$$M_N = S/(N_0 A) \tag{16}$$

where A is the surface area of one 2-CEES molecule ($\sim 4 \times 10^{-19}$ m^2) and N_0 is Avogadro's constant.

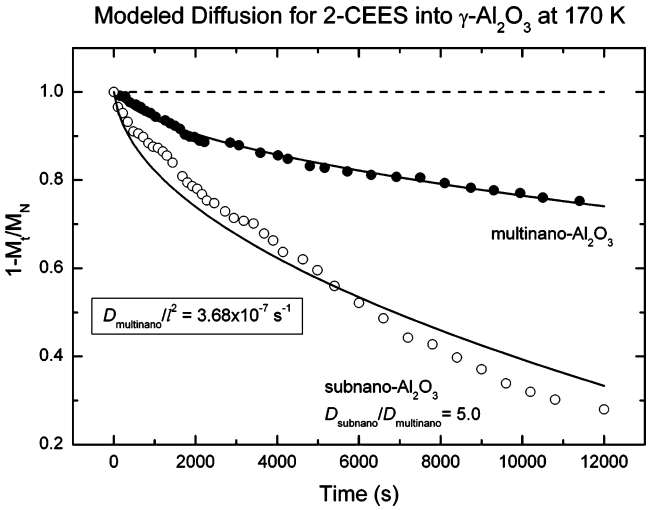

Figure 11. Normalized diffusion amount of 2-CEES into multinano-Al_2O_3 and subnano-Al_2O_3 at 170 K. Symbols are experimental results, and solid lines are the best fit to the experimental data. $D_{multinano}/l^2 = 3.68 \times 10^{-7}\ s^{-1}$. Here l is the thickness of the pressed powder sample.

We have regressed D/l^2 in eq 15 using the experimental data of Figure 3 for 2-CEES diffusion into subnano-Al_2O_3 and multinano-Al_2O_3. The normalized amounts of adsorbed 2-CEES at 170 K from both regression and experiments are shown in Figure 11. Regressed results fit very well with the experiments for multinano-Al_2O_3 and fairly well with the subnano-Al_2O_3. A ratio of $D_{s,subnano}/D_{s,multinano} \approx 5$ was found from the regressed diffusion coefficients at 170 K. This value is in remarkably good agreement with the range of values computed in the previous analysis.

Since the practical temperature for application of these aluminas for adsorption is near 300 K, it is of interest to calculate the diffusivity ratio at the higher temperature. Using eq 5 and assuming $C_{T-sites,multinano} \approx 1.3C_{T-sites,subnano}$ and the observation that $D_{s,subnano}/D_{s,multinano} \approx 5$ at 170 K, we estimate that the ratio $D_{s,subnano}/D_{s,multinano} \approx 2.6$ at 300 K.

V. Summary

The diffusion of the 2-chloroethylethyl sulfide (2-CEES) molecule into two types of γ-Al_2O_3 powders was studied using transmission FTIR spectroscopy, probing the kinetic behavior of isolated Al−OH sites as hydrogen bonding occurs at these trap sites. The temperature dependence and isothermal diffusion experiments show that the diffusion of the 2-CEES molecule into the subnanometer crystallite size (<1 nm) Al_2O_3 powder is more rapid than in the multinanometer (2−3 nm) crystallite size Al_2O_3. A surface diffusion model indicates that the diffusion coefficient, D, on the subnano-Al_2O_3 is ∼5 times larger than that on multinano-Al_2O_3 for the 2-CEES molecule at 170 K.

Acknowledgment. We acknowledge with thanks the support of this work by The Army Research Office and discussion with Dr. Alex Balboa of the Aberdeen Proving Ground. We also thank Dr. Olga Koper and Professor Kenneth Klabunde for providing the two well-characterized γ-Al_2O_3 samples studied here.

References and Notes

(1) Yang, Y.-C.; Szafraniec, L. L.; Beaudry, W. T.; Davis, F. A. *J. Org. Chem.* **1990**, *55*, 3664.
(2) Yang, Y.-C.; Szafraniec, L. L.; Beaudry, W. T.; Ward, J. R. *J. Org. Chem.* **1988**, *53*, 3293.
(3) Wagner, G. W.; Bartram, P. W.; Koper, O.; Klabunde, K. J. *J. Phys. Chem. B* **1999**, *103*, 3225.
(4) Valiullin, R.; Kortunov, P.; Kärger, J.; Timoshenko, V. *J. Phys. Chem. B* **2005**, *109*, 5746.
(5) Valiullin, R.; Kortunov, P.; Kärger, J.; Timoshenko, V. *J. Chem. Phys.* **2004**, *120*, 11804.
(6) Knözinger, H.; Ratnasamy, P. *Catal. Rev. Sci. Eng.* **1978**, *17*, 31.
(7) Peri, J. B.; Hannan, R. B. *J. Phys. Chem.* **1960**, *64*, 1526.
(8) Digne, M.; Sautet, P.; Raybaud, P.; Euzen, P.; Toulhoat, H. *J. Catal.* **2004**, *226*, 54.
(9) Popova, I.; Yates, J. T., Jr. *Langmuir* **1997**, *13*, 6169.
(10) Basila, M. R.; Kantner, T. R.; Rhee, K. H. *J. Phys. Chem.* **1964**, *68*, 3197.
(11) Mawhinney, D. B.; Rossin, J. A.; Gerhart, K.; Yates, J. T., Jr. *Langmuir* **1999**, *15*, 4789.
(12) Basu, P.; Ballinger, T. H.; Yates, J. T., Jr. *Rev. Sci. Instrum.* **1988**, *59*, 1321.
(13) Yates, J. T., Jr. *Experimental Innovations in Surface Science*; Springer-Verlag: New York, 1998.
(14) Kim, S.; Bly, O.; Yates, J. T., Jr. *J. Phys. Chem. B.* **2005**, *109*, 3499.
(15) Ballinger, T. H.; Wong, J. C. S.; Yates, J. T., Jr. *Langmuir* **1992**, *8*, 1676.
(16) Mawhinney, D. B.; Rossin, J. A.; Gerhart, K.; Yates, J. T., Jr. *Langmuir* **2000**, *16*, 2237.
(17) Zawadski, A.; Parsons, S. *Acta Crystallogr., Sect. E* **2004**, *60*, o225.
(18) Duong, D. D. *Adsorption Analysis: Equilibria and Kinetics*; Imperial College Press: Singapore, 1998.
(19) Gomer, R. *Field Emission and Field Ionization*; American Institute of Physics: New York, 1993.
(20) Redhead, P. A. *Vacuum* **1962**, *12*, 203.
(21) Yates, J. T., Jr. *Methods Exp. Phys.* **1985**, *22*, 425.
(22) Crank, J. *The Mathematics of Diffusion*; Oxford University Press: New York, 1975.